Article

Previous Article | Next Article | Table of Contents

Intrinsic Base-Pair Rearrangement in the Hairpin Ribozyme Directs RNA Conformational Sampling and Tertiary Interface Formation

Patrick O. Ochieng, Neil A. White, Michael Feig, and Charles G. Hoogstraten*
Department of Biochemistry and Molecular Biology, Michigan State University, East Lansing, Michigan 48824, United States

J. Phys. Chem. B, **2016**, *120* (42), pp 10885–10898
DOI: 10.1021/acs.jpcb.6b05606
Publication Date (Web): October 5, 2016

*E-mail: cghoogstraten@cns.msu.edu; Telephone: 517-353-3978; Fax: 517-353-9334.

Abstract

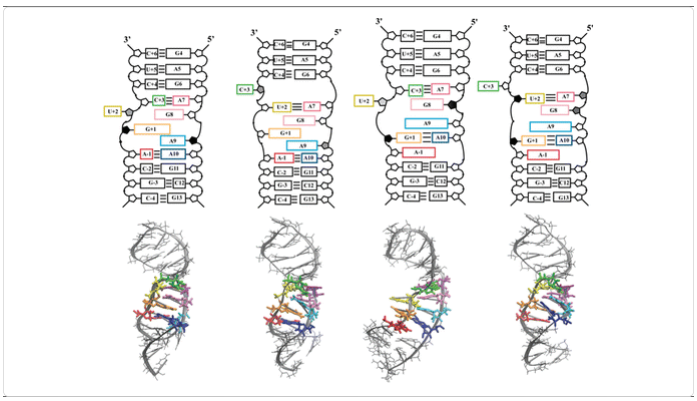

Dynamic fluctuations in RNA structure enable conformational changes that are required for catalysis and recognition. In the hairpin ribozyme, the catalytically active structure is formed as an intricate tertiary interface between two RNA internal loops. Substantial alterations in the structure of each loop are observed upon interface formation, or docking. The very slow on-rate for this relatively tight interaction has led us to hypothesize a double conformational capture mechanism for RNA–RNA recognition. We used extensive molecular dynamics simulations to assess conformational sampling in the undocked form of the loop domain containing the scissile phosphate (loop A). We observed several major accessible conformations with distinctive patterns of hydrogen bonding and base stacking interactions in the active-site internal loop. Several important conformational features characteristic of the docked state were observed in well-populated substates, consistent with the kinetic sampling of docking-competent states by isolated loop A. Our observations suggest a hybrid or multistage binding mechanism, in which initial conformational selection of a docking-competent state is followed by induced-fit adjustment to an in-line, chemically reactive state only after formation of the initial complex with loop B.

Introduction

Recent years have seen an increasing appreciation of the critical role of conformational dynamics in aspects of biomolecular function including enzymatic catalysis, allostery, and molecular recognition.(1-12) In the case of molecular recognition, dynamic aspects of function are often discussed in terms of two useful if oversimplified limiting paradigms. “Induced fit” implies initial binding by the most populated (ground) states of each molecule followed by conformational adjustment within the bound state, whereas “conformational capture” implies equilibrium fluctuations of the binding component to a conformation closely resembling that observed in the complex, with that subpopulation of molecules then being competent for binding upon molecular collision. Experimental and simulation studies aimed at distinguishing conformational-capture and induced-fit mechanisms generally explore the conformations available to the free molecule. The existence of a defined state or measurable population corresponding to a conformation resembling the bound state is taken as evidence for a conformational capture mechanism.

Dynamics may be a particularly important mechanistic aspect of RNA systems, for which the structural features of the ground state can be less favorable for precise programming of function than in analogous protein systems.(13-15) From the early days of the structural biology of RNA in complex with peptides, proteins, and small molecules, stark differences between the conformation of bound and free RNA indicated the general importance of conformational sampling during ligand binding by RNA.(6, 7, 16) In the context of catalytic RNA molecules (ribozymes), a detailed understanding of the how RNA structure and dynamics limit catalytic rates requires an understanding of the subset of molecular conformations that are catalytically competent and how those conformations are sampled within the ground-state ensemble of the system.

Molecular dynamics (MD) simulation and nuclear magnetic resonance (NMR) spectroscopy are powerful and complementary tools for interrogating time scales relevant for the conformational capture process.(17, 18) In the case of RNA, the energy landscape is typically more rugged than for proteins,(19, 20) implying that multiple alternate states, separated by kinetic barriers, may be populated to a significant extent at physiological temperatures. This has hindered past efforts to fully characterize the conformational dynamics of RNA and in particular to explore to what extent conformational capture or induced fit processes are at play in RNA–RNA interactions.

In this work, we have used the hairpin ribozyme, a paradigmatic member of the small, self-cleaving class of catalytic RNAs,(21-26) as a model system to study the role of RNA dynamics in RNA–RNA tertiary recognition. The two internal loops of this ribozyme interact (dock) in a cation-dependent fashion to form a tightly integrated active structure that cleaves a specific phosphodiester bond within loop A (Figure 1). Constructs in which loops A and B are present in separate molecules and docking takes place in intermolecular fashion show catalytic activity(27, 28) and represent a relatively rare example of intermolecular RNA tertiary structure formation uncoupled from the formation or breakage of helical secondary structure. Full ribozyme activity is observed if the presumed physiological ligand Mg^{2+} is replaced by the exchange-inert $Co(NH_3)_6^{3+}$, implying a lack of direct metal-ion participation in the chemical steps of catalysis.(29-31) The mechanism of the ribozyme has been studied intensively via experiment and modeling.(20, 22-24, 32-62) NMR structural models of the isolated loops have been determined, as have numerous crystal structures of the docked form in the presence and absence of the native four-way RNA junction.(63-71) The catalytic core of the docked form reveals a network of stacking and hydrogen-bonding interactions within the active site that orient the reactive phosphate in the in-line orientation for an S_N2-type nucleophilic attack mechanism and position nucleotide base functional groups to facilitate catalytic chemistry (Figure 1C).(65, 66, 72, 73) Significant structural rearrangements of both loops are observed upon formation of the intricate docking interface, as represented schematically in Figure 2.(41, 65, 72, 74, 75) For example, U+2 and U41 are extrahelical in the free forms of loop A and loop B, respectively, but take part in G8:U+2 and A22:U41 base-pairs in the docked form. In a critical interloop interaction, residue G+1 adjacent to the scissile phosphodiester in loop A forms an interdomain Watson–Crick base-pair with C25 in loop B via disruption of the G+1:A9 and C25:U37 noncanonical base pairs in the individual loop structures.

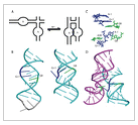

Figure 1. Docking transition in the hairpin ribozyme. (A) Schematic of the native four-way junction sequence showing internal loops A and B and the metal-driven docking event that forms the catalytically active structure. (B) Comparison of a model of the wild-type loop A in isolation based on the solution structure of the A-1C mutant (left; see text) with loop A as it exists in complex with loop B in a crystal structure of the junctionless ribozyme (PDB code 2OUE; right).(68) The GAAA tetraloop is shaded in gray. (C) Comparison of the active-site groups in solution (top) and crystal (bottom) states, as in B. Cleavage occurs at the phosphodiester connecting A-1 and G+1. (D) Complete crystal structure of the docked ribozyme (PDB 2OUE)(68) with loop B in purple. Individual nucleotide colors are consistent among panels B, C, and D. Figure prepared with Pymol.(119)

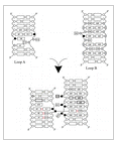

Figure 2. Schematic representation of the solution NMR structures of isolated loops A and B as well as the crystallographic form of the docked structure. Pentagons represent ribose sugar groups and boxes represent nucleotide bases. Ribose puckers are indicated as follows: C3′-endo (open), C2′-endo (solid), or equilibrium (gray) (NMR data only). The double-boxed residues form a structured binding pocket for U42. Red lines represent newly formed base-pairs in the docked structure (PDB 1M5K).(65)

Intermolecular on- and off-rates for ribozyme docking in the absence of junction sequences reveal a high-affinity but unusually slow docking process between loop A and loop B.(76) In combination with the sharp structural contrast between the free and docked forms of each loop, this slow association rate has suggested a “double conformational capture” mechanism for RNA–RNA recognition, in which only collisions between molecules independently sampling minor docking-competent states are productive for complex formation. This model predicts that isolated loops A and B may both sample conformations with an increased resemblance to their respective docked forms. In the present report, we probe the conformational sampling of the loop A domain of the hairpin ribozyme as an initial step to understanding the active-site dynamics in this RNA system. Unconstrained molecular dynamics simulations of isolated loop A are used to map out the conformational ensemble sampled by the system in the absence of its binding partner. We pay particular attention to sampling of features associated with the docked state and potential docking-competent conformations. The results both support and refine simple ideas of conformational capture in this system, suggesting a potential multistage mechanism for the formation of RNA tertiary interactions.

Methods

Unconstrained Molecular Dynamics (MD) Simulations

Initial molecular dynamics (MD) simulations in two different force fields were carried out from the solution structure of an A-1 to C mutant (A-1C) loop A determined by Cai and Tinoco(63) and denoted LpA. Coordinates were kindly supplied by Ignacio Tinoco Jr. For wild-type loop A production simulations, stem 1 was extended with a GAAA tetraloop derived from a theophylline-theophylline aptamer RNA structure (PDB code 1O15)(77) and residue C-1 was mutated to A-1

using the MMTSB Tool Set(78) to restore the native sequence. One G-C base pair was added at the distal end of stem II to enhance stability during the simulation time. The resulting construct is denoted hpA. The two constructs are illustrated, along with the numbering used in this article, in Figure 3 and the key features of each set of simulations are given in Table 1. Detailed calculational protocols are given in the Supporting Information.

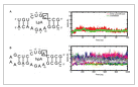

Figure 3. Secondary structure representation of loop A constructs used in this work, along with heavy atom RMSD profiles from the solution-structure mutant sequence (LpA) (A) and wildtype loop A (hpA) (B). In A, the red and green profiles represent Amber param99-bsc0 and CHARMM36 simulations, respectively. In B the colors represent replicate simulations with CHARMM36.

Table 1. Summary of Molecular Dynamics Simulations of Loop A Constructs

simulation	LpA[a]	LpA[a]	hpA[b]
length of simulation (ns)	100	100	1,000
force field	CHARMM36	Amber param99-bsc0	CHARMM36
number of simulations	1	1	20

aLpA denotes explicit solvent simulation on the sequence of the solution structure (Figure 3A) using the indicated force field.
bhpA represents simulation of wildtype loop A construct (shown in Figure 3B). In the text, simulation replicas are denoted hpA1–20.

Markov State Model Generation

Markov state model(79) (MSM) analysis was used to identify and model conformational states and transitions from the hpA simulations using the MSMBuilder 3.5.0 software package.(80) The snapshots from the simulations (about 2,000,000 total saved at 10 ps intervals) were clustered using intramolecular distances between C-2:C4, A-1:N1, G+1:N1, U+2: C4, C+3:C4, C+4:C4, G6:N1, A7:N1, G8:N1, A9:N1, A10:N1, G11:N1 as features since the base pairing configurations of the internal loop residues are the key property of interest that distinguishes different states. 250 clusters were generated for the MSM model to ensure that the conformational variety of the generated ensemble was captured, but the analysis was focused only on the most populated clusters. Continuous-time MSM analysis was then carried out to obtain a kinetic model.

Base-Pair Formation

In order to characterize noncanonical base-pairing in the central loop region, we identified two pairs of atoms between two bases to constitute a base-pair interaction. Using a single atom pair made it difficult to distinguish base-pairing from stacking where an atom pair may also come close. Interactions between both pairs of atoms were simultaneously required to be within 3.5 Å. If multiple alternate base-pairing and/or base-pairs from the same base (out of A7, G8, A9, A10) with two other bases were found to be within the distance cutoff criteria, only the base-pair with the shortest distance was counted.

Other Analyses

Various structural analyses of the simulations were carried out using the MMTSB (Multiscale Modeling Tools for Structural Biology) Tool Set(78) in conjunction with CHARMM. RMSD values were calculated for all heavy atoms excluding the terminal nucleotides due to fraying. Previously reported NMR nuclear Overhauser effect (NOE) distances were calculated from LpA trajectories using the MMTSB Tool Set(78) in conjunction with CHARMM and subsequently averaged.

Results and Discussion

Force Field Choice

The calculations reported in this work are intended to explore the conformational sampling of RNA and the effects of that sampling on tertiary RNA–RNA interface formation, and therefore depend critically on the appropriate behavior of the molecule under the force field used. Thus, we carried out preliminary simulations of the loop A solution structure (LpA) using updated force fields from the Amber and CHARMM families (Amber param99-bsc0(81-83) and CHARMM36,(84-88) respectively) and evaluated whether the resulting trajectories maintained several unusual proton–proton nuclear Overhauser effect (NOE) contacts reported in the system.(63) Both simulations were stable as evidenced by RMSD values averaging about 3 Å from the NMR starting structure during 100 ns of simulation (Figure 3A). As discussed in detail in Supporting Information (see Tables S1 and S2 and Discussion), for these particular questions in the specific loop A system, CHARMM36 performed somewhat better over 100 ns in terms of reproducing experimental sugar puckers and helical parameters and maintaining unusual NOE contacts, and therefore was chosen for production simulations of the wild-type loop A constructs. We note that the current results are not intended as systematic comparisons and should not be taken as bearing on general questions of force field quality or applicability in nucleic acid systems, a topic of much current interest.(89, 90)

Conformational Heterogeneity of Wild-Type Loop A

The wild-type loop A construct (hpA) was modeled based on the mutant loop A NMR structure via conversion of C to A at position −1, interpolation of a GAAA tetraloop to cap Helix II, and a minor extension of Helix I (see Methods). The combined sampling from 20 independent molecular dynamics simulations yielded a total of 20 μs of explicit-solvent MD simulation to describe the conformational ensemble of loop A. The RMSD with respect to the initial structures of the wild-type loop A construct showed generally larger RMSD variations than for the mutant hpA structure (see Figure 3B). Initial inspection revealed an overall preserved hairpin structure where the base-pairing in the stem regions is largely conserved but with significant conformational dynamics in the internal loop region.

To further describe the conformational ensemble, Markov state analysis was carried out based on variations in base–base distances within the central loop region (see Methods). We constructed the Markov state model from clustering into 250 microstates. The large number of clusters was necessary to fully capture the variations in the conformational ensemble. If a smaller number of clusters was used, we found that a majority of comparatively more similar snapshots was combined into a single cluster while the remaining clusters captured small populations of

conformations that were further away in conformational space. Although other clustering techniques such as hierarchical clustering can in principle deal better with unevenly distributed data, we opted here for simply generating a larger number of clusters and then focusing the analysis on the most populated states.

We classified the MSM states based on their base-pairing and presence of extra-helical bases. Base-pairing was analyzed with respect to A10, A9, G8, and A7 based on interaction-forming interbase atoms being closer than 3.5 Å. Initial analysis indicated the possibility for A-1 or G+1 pairing with A10 or A9 as well as U+2 or C+3 pairing with G8 or A7. For a given base-pair, we observed one to three alternate base-pairing configurations when base-pair formation was determined as described in the Methods section. For convenience, the resulting base-pairing in the central loop was encoded using an eight-letter notation to describe the predominant base-pairing with respect to A10, A9, G8, and A7 in a given state. Base-pairing with A10 was either A-1:A10 (“AA”) or G+1:A10 (“GA”); pairing with A9 was either A-1:A9 (“aa”) or G+1:A9 (“ga”); pairing with G8 was U+2:G8 (“ug”) or C+3:G8 (“cg”); and pairing with A7 was U+2:A7 (“UA”) or C+3:A7 (“CA”). In the eight-letter notation, ‘AAga...CA’, for example, means A-1:A10, G+1:A9, and C+3:A7 base pairing while G8 was unpaired. “XX” or ‘xx was used to describe equal or near-equal populations of alternate base-pairing for a given base. When bases were left unpaired, they either stacked or, in a subset of cases, the G+1, U+2, C+3, G8, and A9 bases flipped out of the helical structures to varying degrees. For some analyses, base pairs adjoining the Watson–Crick helices were used to define four major base-pairing configurations (AA/CA, AA/UA, GA/CA, and GA/UA, in the same shorthand)

The 40 most populated states along with their classification and extra-helical bases are listed in Table S3. These 40 states collectively capture 75% of all of the snapshots generated in the simulations. A full list with more detailed conformational data for all 250 states is deposited separately in the Supporting Information. The majority of base-pairing in the central loop involves A10 (AA or GA) or A7 (UA or CA). The most populated states cover all combinations of AA/CA, GA/CA, AA/UA, and GA/UA as well as states where either A10 or A7 or both were not base-paired to a significant extent according to our criteria. AA/CA is the major conformer since 50% cumulative population of all states classified as AA/CA, followed by AA/UA (22%), GA/UA (6%), and GA/CA (4%). In the remaining states (covering 18% of the snapshots), either A10 or A7 or both were not base-paired to a significant degree. Within each major conformer, substates are distinguished with respect to the conformation of the remaining nucleotides. In many states, at least one of the bases is extra-helical for at least half of the snapshots (Table S3). The extra-helical bases were often fully flipped out extending away from the helix but in some cases the bases remained closer to one of the grooves and occasionally interacted partially with other non-neighboring bases. Figure 4 shows representative structures for the most populated clusters in each of the four major states along with schematic illustrations of the configuration of the bases in the central loop region.

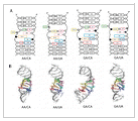

Figure 4. Schematic representations (A) and corresponding structural renderings (B) of representative structures for the four major states AA/CA (#175), AA/UA (#123), GA/CA (#201), and GA/UA (#181). Schematic representations adopt the nomenclature used in Figure 2. In the 3D structures, the central base pairs are colored as follows: A-1 (red), G+1 (orange), U+2 (yellow), C+3 (green), A7 (magenta), G8 (mauve), A9 (cyan), A10 (blue). Figure prepared with VMD.(120)

To more quantitatively analyze the base-pairing, we report in Table 2 the percentages of noncanonical base-pair formation in all of the generated snapshots as a function of the major base-pair conformer. Since this analysis considers each snapshot separately, the percentages of AA/CA, AA/UA, GA/CA, and GA/UA base-pairing are lower than the percentages of MSM states classified based on predominant base-pairing exhibited in each state. It can be seen that in addition to the major A-1:A10/G+1:A10 and C+3:A7/U+2:A7 base-pairs, other noncanonical base-pairs involving A-1:A9, U+2:G8, G+1:A9, and C+3:G8 were also sampled.

Table 2. Sampling of Noncanonical Base-Pairing Interactions in Wild-Type Loop A[a]

	AA/CA	AA/UA	GA/CA	GA/UA	Other
% present in snapshots	24.51 (2.0)	16.05 (1.3)	3.93 (0.6)	3.75 (1.5)	51.77 (0.1)
base pairs present in the docked state					
A-1:A9	0.02	1.04	0.00	1.48	5.78
N3-H6x; H2-N7	0.02 (0.01)	1.04 (0.08)	0.00	1.48 (2.30)	5.78 (1.5)
U+2:G8	8.24	0.98	0.53	0.21	4.25
O4-H2x; H5-H2x	7.02 (0.5)	0.56 (0.1)	0.49 (0.2)	0.12 (0.0)	3.17 (0.4)
O4-H2x; H3-H2x	0.22 (0.0)	0.42 (0.1)	0.04 (0.0)	0.09 (0.0)	1.08 (0.1)
C+3:A7	100[b]	0	100[b]		13.40
H4x-N1; N3-H2	40.99 (4.2)		15.25 (9.3)		2.03 (0.6)
H4x-N3; H5-H2	59.01 (4.2)		84.75 (9.3)		11.37 (2.0)
base pairs not present in the docked state					
A-1:A10	100[b]	100[b]	0[b]	0[b]	45.65
N3-H6x; H2-N7	89.04 (4.8)	92.73 (1.3)			53.26 (8.1)
H6x-N1; N1-H2	8.54 (3.4)	4.00 (0.8)			1.73 (0.6)
N1-H6x; H2-N1	2.41 (1.4)	3.27 (0.5)			0.68 (0.0)
G+1:A10	0[b]	0[b]	100[b]	100[b]	5.74
H2x-N7; N3-H6x			48.27 (19.2)	99.06 (0.5)	5.36 (2.5)
N3-H2; H2x-N1			51.73 (0.5)	0.94 (0.5)	0.38 (0.1)
G+1:A9	16.58	7.32	9.95	5.41	21.43
H2x-N7; N3-H6x	13.57 (6.8)	7.32 (0.6)	9.95 (7.6)	5.41 (1.0)	19.22 (8.1)
N7-H8; H8-N7	3.01 (1.9)	0.00	0.00	0.00	2.21 (1.5)
C+3:G8	3.79	0.01	0.74	0.00	10.07
O2-H2x; N3-H1	3.79 (1.0)	0.01 (0.0)	0.74 (0.5)	0.00	10.07 (4.9)
U+2:A7	0[b]	100[b]	0[b]	100[b]	17.26
H3-N1; O4-H6x		73.00 (17.7)		45.90 (24.8)	13.71 (1.6)
H3-N7; O2-H6x		27.00 (17.7)		54.10 (24.8)	3.55 (2.6)

aA distance cutoff of 3.5 Å was applied to consider base-pair formation based on the indicated pairs of atoms. Values given in parentheses reflect statistical errors based on block analysis comparing the first and second half of the trajectories.
bInteraction present (or not) by definition in the listed conformer.

Base flipping and sugar pucker preferences for each central loop residue are given in Table 3. Some loop residues showed extra-helical base flipping that correlated with sugar pucker transitions. Specifically, residues G8, A9, G+1, U+2, and C+3 reported C2′/C3′-endo mixed sugar puckers as well as base-flipping (Table S3) that varied in concert between conformations. Similar base-flipping with mixed pseudorotation state has been observed in other systems.(91) The degree of base flipping and correlated C2′-endo sugar puckering varied as a function of the major base-pairing conformer. In the AA/CA conformations, A9 and U+2 were flipped out for about a third of the time each and G8 was also flipped out in about 9% of the snapshots. In AA/UA, A9 and C+3 were seen extra-helical in a significant portion of the snapshots. In the minor state GA/CA, by contrast, G8 and U+2 were seen extra-helical, whereas in GA/UA conformers, only C+3 was seen extra-helical for significant amounts of time.

Table 3. Conformational Dynamics of Loop Residues During Major States of hpA Simulations

residue	state	% C2′-endo[a]	% C3′-endo[b]	% base extra-helical[c]
A7	AA/CA	0.0	91.0 (0.1)	0.0
	AA/UA	0.0	92.9 (0.7)	0.1 (0.0)
	GA/CA	0.0	91.8 (0.4)	0.0
	GA/UA	0.0	94.4 (1.1)	0.0
	other	0.0	90.4 (0.3)	0.3 (0.1)
G8	AA/CA	5.6 (4.0)	83.2 (4.7)	8.7 (7.2)
	AA/UA	5.2 (0.2)	83.0 (2.7)	0.0 (0.0)
	GA/CA	4.6 (4.5)	84.4 (5.9)	7.1 (7.0)
	GA/UA	6.8 (6.8)	78.1 (5.7)	0.0 (0.0)
	other	7.2 (4.0)	80.4 (4.3)	10.8 (7.9)
A9	AA/CA	23.5 (5.8)	59.8 (5.5)	28.1 (0.2)
	AA/UA	16.9 (8.4)	69.0 (8.5)	32.2 (7.8)
	GA/CA	0.1 (0.0)	78.0 (5.7)	2.4 (0.1)
	GA/UA	1.3 (1.3)	78.8 (3.2)	2.2 (0.2)
	other	20.0 (6.3)	61.6 (6.3)	15.6 (1.0)
A-1	AA/CA	0.0	91.4 (0.2)	0.0
	AA/UA	0.0	91.0 (0.3)	0.0
	GA/CA	0.4 (0.4)	89.9 (0.4)	0.0
	GA/UA	0.0	91.2 (0.7)	0.0
	other	0.1 (0.0)	90.1 (0.3)	0.0
G+1	AA/CA	8.3 (2.4)	82.6 (1.9)	0.9 (0.8)
	AA/UA	25.5 (4.6)	53.9 (9.5)	0.3 (0.2)
	GA/CA	3.7 (0.3)	84.2 (1.8)	0.0
	GA/UA	34.1 (15.4)	47.5 (18.1)	0.0
	other	17.4 (6.0)	68.9 (6.7)	6.9 (5.1)
U+2	AA/CA	11.0 (0.2)	77.2 (0.3)	31.3 (0.6)
	AA/UA	36.5 (9.2)	46.4 (12.4)	0.0
	GA/CA	6.4 (2.1)	87.2 (2.8)	16.0 (8.9)
	GA/UA	55.9 (15.0)	28.6 (16.2)	0.0
	other	16.1 (6.0)	72.5 (6.7)	17.0 (2.8)
C+3	AA/CA	0.0	91.6 (0.0)	0.1 (0.0)
	AA/UA	3.6 (0.5)	87.3 (0.8)	57.2 (11.7)
	GA/CA	0.0	93.4 (0.6)	0.0
	GA/UA	2.0 (0.4)	88.7 (0.4)	34.1 (19.1)
	other	4.0 (1.0)	87.1 (1.4)	23.2 (0.2)

aC2′-endo has sugar pucker angles of 144–180°.

bC3′-endo has sugar pucker angles of 0–36°.

cBase flipping when N1 (guanine/adenine) or N3 (cytosine/uracil) was not within 5 Å distance from any base atom of either neighboring base or the respective base-pair forming base(s). Underlined values represent conformations of the docked state, as observed in multiple crystal structures of wildtype loop sequences in either four-way junction or junctionless forms (PDB 1M5K, 2D2K, 1X9K, 1X9C, 2OUE).(65, 67, 68) Errors based on block analysis from comparing first and second half of the trajectories are given in parentheses.

Conformational Transitions between Major States

The relatively long individual simulations (each over 1 μs) allowed the observation of structural transitions among different major conformations. Although no individual simulation sampled all of the states, the combination of all 20 simulations allowed the construction of a comprehensive kinetic Markov state model for the system. The model was constructed from all 250 microstates, but for clarity we again focused analysis on the 40 most populated states. The resulting network of states is shown in Figure 5. States within the four major conformers are highly connected, often with rapid interconversion on nanosecond time scales. However, there are also extensive connections between different major conformers. Only two states are not directly connected within this forty-state subset (#5 and #174), although these states become connected to the rest of the network when the full set of 250 microstates is considered. The AA/CA and AA/UA conformers have similar free energies and a similar number of states. The most populated AA/UA state (#123) is only slightly higher in free energy than the most populated AA/CA state (#175). Based on the kinetic model, transitions between the most populated AA/CA and AA/UA states appear to require intermediate transitions via slightly elevated states (for example #246 or #190) and kinetic barriers on submicrosecond time scales. The less populated GA/UA and GA/CA states are energetically higher but also appear to be accessible on submicrosecond time scales. Taken together, these results suggest that the majority of states on this complex and extensive conformational landscape of loop A should be fully accessible to a single loop A molecule on time scales of 10–100 μs. This is consistent with our previous NMR spin relaxation results in the GCAA tetraloop(92) and the lead-dependent ribozyme,(93) which also suggest that sampling of minor forms of highly structured RNAs often occurs on time scales of tens of microseconds.

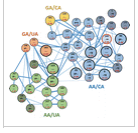

Figure 5. Markov state model for 40 most populated states shown as spheres with different radii reflecting their relative population and colored according to their major base-pairing conformer. For each state the index is given along with the minor base-pair conformation involving A9 and G8 and the relative free energy in kcal/mol based on population size relative to the most populated state. Connections between states are based on estimated rates of at least 10 μs^{-1}. Faster rates are reflected by thicker edges with the thickest edges corresponding to rates exceeding 1 ns^{-1}.

Features of the Docked State Are Sampled in Trajectories of Isolated Loop A

The most populated structure adopted by loop A in isolation(63) is quite distinct from that found in the activated conformation formed by the loop A–loop B interface.(65) A key prediction of our double conformational capture model for tertiary structure formation is that loop A in isolation samples docking-competent conformations that contain structurally important features of the docked state. Important structural transitions between the free and docked states for loop A include the extrusion of G+1 from the helix for base-pairing with C25 of loop B, transitions of sugar pucker to C3′-endo at G8 and G+1, and the formation of noncanonical U+2:G8 and C+3:A7 base pairs. In addition, the cleavage-competent conformation at the active site is associated with a reorientation of the A-1 ribose to a C2′-endo conformation that favors the in-line attack state along with a base pairing of A-1 to A9 (Figure 2). In our unconstrained simulations, the predominant conformation (AA/CA) is defined by the C+3:A7 base pair present in docked loop A. U+2:G8 base pairing is seen rarely although the largest fraction (around 8%) is again seen for the AA/CA conformer (see Table 2). Sugar puckering of G8 is generally in C3′-endo form and for G+1, C3′-endo sugar puckers are dominant for AA/CA whereas their population is reduced in favor of C2′-endo for AA/UA, the second most populated major conformer in our simulations. A-1:A9 base-pairing is also seen in our simulations, but it is very rare for AA/CA (~0%) and AA/UA (1%) and seen most often (in about 5% of the snapshots) when either A10 or A7 or both are not base-paired. Base flipping at G+1 is seen a small percentage of the time, largely in combination with less-common base-pairing patterns (Table 3). Global comparisons between our observed conformers and the docked form of loop A based on root-mean-square deviations (RMSD) to the docked loop A structure (based on PDB ID 1M5K(65)) also showed closer approaches for AA/CA states than for AA/UA states (see Table S3) including the microstate with the overall lowest average RMSD of 2.78 Å (#249). Analyzing all of the snapshots individually, we found the closest approach to the docked state in our simulations to be a snapshot from state #249 displaying a RMSD of 2.1 Å. As shown in Figure 5, #249 is well-connected kinetically with other AA/CA substates but relatively far from the alternate AA/UA, GA/CA, and GA/UA conformers. The state with the second closest approach to the docked conformation, #47, is similar to #249 and kinetically connected in the MSM. To summarize, many important features of the docked state, and thus of presumed docking-competent states of isolated loop A, are observed in our simulations, and sub-states are observed that resemble the docked conformation much more so than the most-populated states do. On the current time scale, states in which the full panoply of structural shifts between the free and docked structures have simultaneously engaged are not found by the clustering algorithm. Given the very slow time scale of the docking reaction itself, it may be that such forms would emerge over tens to hundreds of microseconds of dynamics, as has been suggested by NMR results in other structured RNA systems.(92-94)

Conformation of the Reactive Groups

Figure 6 compares a representative structure from AA/CA microstate #249 to the docked loop A structure. Overall, the structures align well but there are differences in the central loop region where only the C+3:A7 base-pairing matches very well with the docked form. U+2:G8 is paired but G8 is rotated in from the docked structure. G+1:A9 is also paired in contrast to the docked form where G+1 is extrahelical. Finally, A-1:A10 is also paired in the simulation snapshot whereas A-1 is actually well above the plane of A10 in the docked structures where it is not able to form the A10:A-1 base-pair.

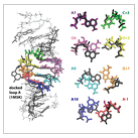

Figure 6. Sampling of features of the docked conformation of loop A provides initial evidence of conformational capture mechanism. Structural comparison between the docked loop A crystal structure (black; PDB 1M5K)(65) with the simulated microstate that most closely resembles the docked loop A structure (microstate #249). The overall structure is compared on the left whereas individual central loop base pairs are compared on the right. Central loop bases for the simulated microstate are colored as in Figure 4. Figure prepared with VMD.(120)

The conformation of A-1 is important since it prepares the reactive groups for “in-line” attack of the A-1 2′-hydroxyl on the adjacent phosphodiester bond with departure of the G+1 5′-oxygen. In a wide variety of crystal structures of the docked conformation of the ribozyme, the A-1 ribose is commonly held in in-line conformation via a cluster of nearby interactions including an A-1:A9 base pair.(65, 67-69, 71, 95-97) Adoption of the in-line geometry is seen in both 2′-hydroxy and 2′-O-methyl versions of the ribozyme,(68) and is closely correlated with adoption of the C2′-endo conformation at A-1.(69) In the simulations reported here, although A-1:A9 base pairs are rarely observed (see above), we do see a subset of conformations in which attack angles approach 180°, sometimes accompanied by close O2′-P distances (Figure 7). Of over 500,000 snapshots analyzed, five (0.001%) show attack angles greater than 150° and O2′-P distances less than 3.2 Å, common criteria for a true in-line attack conformation.(98) These snapshots arise from AA/CA substates #204, #44, and #177, which also account for the majority of snapshots displaying attack angles >120° regardless of distance (see Figure 7 and Supporting Information). Thus, our simulations indicate that isolated loop A is capable of adopting catalytically competent in-line conformations at the nucleophilic reaction center, but samples those conformations a vanishingly small fraction of the time in the absence of the loop B binding partner. In the presence of loop B, by contrast, crystallographic analysis consistently demonstrates the adoption of such geometries.(65, 67-69, 71, 95) Taken together, our observations suggest a multistage interaction mechanism for loop A whereby initial conformational selection of a docking-competent state containing some features of the docked state is followed by adjustment to an in-line, chemically reactive state only after formation of the initial complex with loop B.

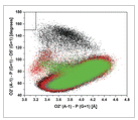

Figure 7. Coordinates associated with in-line attack conformation in simulations of loop A for AA/CA (black), AA/UA (red), GA/UA (blue), and GA/CA (green) states. Dotted lines indicate the small subset of conformations with attack angle >150° and O2′-P distance <3.2 Å (see text).

In complementary work to that reported here, molecular dynamics calculations on the docked state have helped throw light on the determinants for the ultimate formation of chemically reactive states in the hairpin ribozyme.(62) Intriguingly, recent results have supported a late-stage rearrangement

of reactive groups in the full-length hammerhead ribozyme that parallels our proposed multistage mechanism in the hairpin system.(99) In addition, recent simulations comparing the structure of the twister ribozyme in the presence and absence of crystal-packing constraints have suggested that interactions within the crystallographic unit cell may have fortuitously trapped that self-cleaving RNA prior to final rearrangement to in-line attack conformation as well.(100) In the hepatitis delta ribozyme, simulations have revealed a complicated interplay among conformational sampling and the binding of catalytically critical metal ions,(101) in a mechanism with some parallels to the dynamics-enabled binding of loop B postulated here for the hairpin loop A system. A similar mechanism has also recently been observed in U1A-RNA molecular recognition, wherein U1A helix C is observed to reorient to a bound-like state in the absence of RNA.(102) The conformational capture of binding-competent states followed by an induced-fit adjustment to the structurally observable bound conformation may be a general feature of macromolecular recognition by flexible RNA molecules.

The presence of a GNRA tetraloop in our construct provided a useful control for assessing observed dynamics within the internal loop. The GAAA tetraloop incorporated in our RNA remained structurally stable over the simulation time, consistent with NMR studies(103) and with other simulations done at similar temperatures.(104, 105) This suggests that our observations provide a realistic behavior of this independently folded RNA. Previous studies of RNA systems have observed the formation of AA and GA sheared-type noncanonical base-pairing within internal loops,(106-109) consistent with the alternative A-1:A10 and G+1:A10 pairings observed in our conformers. Published simulations of the full docked ribozyme(52, 54, 56, 57, 60, 62) showed dynamics within loop A of limited scope with conservation of most features of the crystal structure, suggesting that the flexibility of isolated loop A observed in our simulations is necessary for its preorganization prior to formation of the less-flexible docked form.

Conformational Dynamics and Tertiary Structure Formation

The dynamic properties of RNA enable the diverse structural rearrangements associated with transitioning kinetic barriers and sampling functionally competent structures.(18, 110, 111) For example, internal motions leading to the melting of base-pairs near the internal loop of HIV-1 stem loop 1 have been observed using NMR that resemble a secondary structural transition associated with viral maturation.(112) In the case of the hairpin ribozyme, dramatic structural shifts are observed for each of the two active-site internal loops upon formation of the catalytically active docked state, leading to an intricate RNA tertiary interface that does not rely on stabilization from canonical double helices. Interestingly, cross-linking experiments have shown the formation of multiple functional folds of the hairpin ribozyme under different metal ion conditions, suggesting the energetic accessibility of multiple conformational states centered at the U+2 and C+3 residues.(113, 114) In the simulations reported here, base-flipping dynamics at these same two residues are key features of the sampling of varying conformational states (Figure 4).

Our group's SPR analysis of intermolecular loop–loop docking showed a submicromolar binding interaction that nevertheless displayed unusually slow docking on-rates on the order of 2000 M^{-1} s^{-1}.(76) Based in part on this observation, we hypothesized that the formation of tertiary structure in the hairpin ribozyme may be described as a "double conformational capture" transition, predicting that both internal loops independently sample activated states resembling, in whole or in part, their docked conformation. The assessment of equilibrium fluctuations of loop A in this work provides an important initial step toward a detailed elaboration and testing of this hypothesis. Using unbiased explicit solvent simulations, we identified a surprisingly complex conformational energy landscape with four major conformations, distinguished by alternative noncanonical base-pairing and stacking interactions within the internal loop of loop A, as well as numerous minor states within each of the major conformers. Transitions between different states are primarily facilitated by the dynamics of the bases U+2, C+3, and A9. These residues are strongly conserved in the hairpin, and have previously been implicated in facilitating docking between loop A and loop B.(115) We estimate kinetic barriers on microsecond time scales between the major conformers and submicrosecond kinetics for transitions within each conformer. This reinforces the idea of an RNA energy landscape that consists of many competing local minima and complex transition pathway networks.(92, 116, 117) The observed equilibrium fluctuations provide pathways for accessing a variety of conformational wells connecting the highly populated conformations. In the case of U+2, line broadening in ^{1}H NMR is consistent with substantial microsecond/millisecond scale dynamics,(63) implying that this residue indeed undergoes conformational exchange. Our results indicate that this exchange is predominantly base-flipping facilitated by pucker exchange. Scalar coupling analysis also indicated a mixture of sugar pucker populations for both U+2 and C+3 (Figure 2),(63) further supporting the presence of exchanging conformers at these two residues. The current results provide detailed predictions for the dynamic properties of the loop on microsecond time scales, including fast time scale motions of base and/or sugar residues at U+2, C+3, and A9, ribose reorientation modes at G+1 and G8, and sampling of globally reorganized noncanonical base-pairing patterns and overall loop configurations on time scales of microseconds or longer. We are now engaged in testing these concrete predictions using NMR spin-relaxation and specific isotope labeling technologies.(92, 93, 118)

In the case of loop B, an NMR structural study by the Feigon group reported substantial averaging of scalar coupling constants diagnostic of sugar pucker conformation as well as the existence of mutually inconsistent proton–proton nuclear Overhauser effect (NOE) contacts, consistent with the existence of multiple conformations for the internal loop.(64) Some of the NOEs deemed inconsistent with the most populated state for the isolated loop in solution were suggested to be more consistent with the docked state.(65, 72) Although inconsistent NOEs are not definitive probes of molecular dynamics, these observations provide preliminary support for possible conformational sampling in loop B complementary to that observed here for loop A. Taken together with these data, the formation of multiple kinetic substates in loop A in the current simulations presents strong initial evidence for conformational sampling as a way of facilitating the formation of complex RNA tertiary structures and for the proposed double conformational capture mechanism in the hairpin system. The observation of multiple conformations and internal loop dynamics in loop A of the hairpin ribozyme lays down a framework for understanding the complex nature of RNA dynamics and their role in preorganizing RNA for recognition events within a rugged energy landscape.

Conclusions

In the work reported here, a series of unbiased microsecond MD simulations was used to determine conformational heterogeneity in RNA based on alternate base-pairing within a subset of residues in the loop region of domain A of the hairpin ribozyme. Four major conformers, as defined by the presence of common noncanonical base pairs within the internal loop, were observed, with substantial kinetic microheterogeneity present within each major state. In the simulations, the different conformations were connected via an extensive transition network with individual transitions between microstates on submicrosecond time scales and transitions between major conformers estimated to occur on microsecond time scales. Base and backbone dynamics play an important role in alternate base-pair formation and subsequent conformational sampling in loop A, suggesting that conformational sampling in loop A RNA is a key strategy to avoiding the trapping of this ribozyme domain in a nonfunctional conformation.

Many important features of the crystallographically observed bound conformation were sampled in the various major states and sub-states of the simulations. By contrast, the features of the in-line conformation of reactive groups, and the interactions that support it, were observed to quantitatively insignificant extents in the present simulations. A unified interpretation of these observations is a hybrid, multistage docking mechanism in which conformational sampling within the free loop A creates a docking-competent state or set of states present at low population. Collisions of docking-competent loop B with this population of loop A molecules results in an initial docked complex. Final readjustments of the scissile phosphodiester and its immediate surroundings then result in substantial population of the crystallographically observed, catalytically competent state. From this standpoint, it is interesting that, even for the exchange-inert complex cobalt hexammine, comparisons of the metal dependence of docking with that for ribozyme cleavage suggested that additional metal ion(s) played required roles in the ribozyme mechanism beyond driving formation of the docked state.(76) One intriguing possibility for this additional function of polyvalent cations is facilitation of just such a final conformational adjustment following the formation of the tertiary interface.

Supporting Information

The Supporting Information is available free of charge on the ACS Publications website at DOI: 10.1021/acs.jpcb.6b05606.

- Detailed calculational methods, three data tables, and associated discussion containing a comparison of unusual NOE distances and helical parameters between CHARMM and Amber simulations (PDF)
- Spreadsheet of base pairs and other conformational features characteristic of each of the 250 conformational sub-states (XLSX)

PDF	MS Excel
» jp6b05606_si_001.pdf (179.76 kB)	» jp6b05606_si_002.xlsx (80.66 kB)

Intrinsic Base-Pair Rearrangement in the Hairpin Ribozyme Directs RNA Conformational Sampling and Tertiary Interface Formation

Showing 1/2: jp6b05606_si_001.pdf

SUPPORTING MATERIAL

for

Intrinsic Base-Pair Rearrangement in the Hairpin Ribozyme Directs RNA Conformational Sampling and Tertiary Interface Formation

Patrick O. Ochieng, Neil A. White, Michael Feig, Charles G. Hoogstraten

Department of Biochemistry and Molecular Biology

Michigan State University, East Lansing, Michigan 48824 USA

The authors declare no competing financial interest.

Acknowledgment

The authors gratefully acknowledge Prof. Ignacio Tinoco Jr. for providing the coordinates for the loop A solution structure and Dr. Monika Sharma, Dr. Vahid Mirjalili, Dr. Parimal Kar, and Dr. Beibei Wang for their technical support and useful discussions. We also thank the National Institutes of Health (NIH) (GM069742 to C.G.H. and GM092949 and GM084953 to M.F.) and the National Science Foundation (MCB1413356 to C.G.H. and MCB1330560 to M.F.) for funding.

References

This article references 120 other publications.

1. Karplus, M.Aspects of Protein Reaction Dynamics: Deviations From Simple Behavior *J. Phys. Chem. B* **2000**, 104, 11– 27, DOI: 10.1021/jp993555t [ACS Full Text], [CAS]
2. Hammes-Schiffer, S.Impact of Enzyme Motion on Activity *Biochemistry* **2002**, 41, 13335– 13343, DOI: 10.1021/bi0267137 [ACS Full Text], [CAS]
3. Al-Hashimi, H. M.Dynamics-Based Amplification of RNA Function and Its Characterization by Using NMR Spectroscopy *ChemBioChem* **2005**, 6, 1506– 1519, DOI: 10.1002/cbic.200500002 [CrossRef], [PubMed], [CAS]
4. Kern, D.; Zuiderweg, E. R.The Role of Dynamics in Allosteric Regulation *Curr. Opin. Struct. Biol.* **2003**, 13, 748– 757, DOI: 10.1016/j.sbi.2003.10.008 [CrossRef], [PubMed], [CAS]
5. Wolf-Watz, M.; Thai, V.; Henzler-Wildman, K.; Hadjipavlou, G.; Eisenmesser, E. Z.; Kern, D.Linkage Between Dynamics and Catalysis in a Thermophilic-Mesophilic Enzyme Pair *Nat. Struct. Mol. Biol.* **2004**, 11, 945– 949, DOI: 10.1038/nsmb821 [CrossRef], [PubMed], [CAS]
6. Williamson, J. R.Induced Fit in RNA-Protein Recognition *Nat. Struct. Biol.* **2000**, 7, 834– 837, DOI: 10.1038/79575 [CrossRef], [PubMed], [CAS]
7. Leulliot, N.; Varani, G.Current Topics in RNA-Protein Recognition: Control of Specificity and Biological Function Through Induced Fit and Conformational Capture *Biochemistry* **2001**, 40, 7947– 7956, DOI: 10.1021/bi010680y [ACS Full Text], [CAS]
8. Perez-Canadillas, J. M.; Varani, G.Recent Advances in RNA-Protein Recognition *Curr. Opin. Struct. Biol.* **2001**, 11, 53– 58, DOI: 10.1016/S0959-440X(00)00164-0 [CrossRef], [PubMed], [CAS]
9. Al Hashimi, H. M.; Walter, N. G.RNA Dynamics: It Is About Time *Curr. Opin. Struct. Biol.* **2008**, 18, 321– 329, DOI: 10.1016/j.sbi.2008.04.004 [CrossRef], [PubMed], [CAS]
10. Walter, N. G.The Blessing and Curse of RNA Dynamics: Past, Present, and Future *Methods* **2009**, 49, 85– 86, DOI: 10.1016/j.ymeth.2009.09.002 [CrossRef], [PubMed], [CAS]
11. Mauldin, R. V.; Lee, A. L.Nuclear Magnetic Resonance Study of the Role of M42 in the Solution Dynamics of Escherichia Coli Dihydrofolate Reductase *Biochemistry* **2010**, 49, 1606– 1615, DOI: 10.1021/bi901798g [ACS Full Text], [CAS]
12. Hall, K. B.RNA in Motion *Curr. Opin. Chem. Biol.* **2008**, 12, 612– 618, DOI: 10.1016/j.cbpa.2008.09.033 [CrossRef], [PubMed], [CAS]
13. Narlikar, G. J.; Herschlag, D.Mechanistic Aspects of Enzymatic Catalysis: Lessons From Comparison of RNA and Protein Enzymes *Annu. Rev. Biochem.* **1997**, 66, 19– 59, DOI: 10.1146/annurev.biochem.66.1.19 [CrossRef], [PubMed], [CAS]
14. Kraut, D. A.; Carroll, K. S.; Herschlag, D.Challenges in Enzyme Mechanism and Energetics *Annu. Rev. Biochem.* **2003**, 72, 517– 571, DOI: 10.1146/annurev.biochem.72.121801.161617 [CrossRef], [PubMed], [CAS]
15. Solomatin, S. V.; Greenfeld, M.; Chu, S.; Herschlag, D.Multiple Native States Reveal Persistent Ruggedness of an RNA Folding Landscape *Nature* **2010**, 463, 681– 684, DOI: 10.1038/nature08717 [CrossRef], [PubMed], [CAS]
16. Rambo, R. P.; Doudna, J. A.Assembly of an Active Group II Intron-Maturase Complex by Protein Dimerization *Biochemistry* **2004**, 43, 6486– 6497, DOI: 10.1021/bi049912u [ACS Full Text], [CAS]
17. Dethoff, E. A.; Hansen, A. L.; Musselman, C.; Watt, E. D.; Andricioaei, I.; Al-Hashimi, H. M.Characterizing Complex Dynamics in the Transactivation Response Element Apical Loop and Motional Correlations With the Bulge by NMR, Molecular Dynamics, and Mutagenesis *Biophys. J.* **2008**, 95, 3906– 3915, DOI: 10.1529/biophysj.108.140285 [CrossRef], [PubMed], [CAS]
18. Frank, A. T.; Stelzer, A. C.; Al-Hashimi, H. M.; Andricioaei, I.Constructing RNA Dynamical Ensembles by Combining MD and Motionally Decoupled NMR RDCs: New Insights into RNA Dynamics and Adaptive Ligand Recognition *Nucleic Acids Res.* **2009**, 37, 3670– 3679, DOI: 10.1093/nar/gkp156 [CrossRef], [PubMed], [CAS]
19. Sosnick, T. R.; Pan, T.RNA Folding: Models and Perspectives *Curr. Opin. Struct. Biol.* **2003**, 13, 309– 316, DOI: 10.1016/S0959-440X(03)00066-6 [CrossRef], [PubMed], [CAS]
20. Pljevaljcic, G.; Klostermeier, D.; Millar, D. P.The Tertiary Structure of the Hairpin Ribozyme Is Formed Through a Slow Conformational Search *Biochemistry* **2005**, 44, 4870– 4876, DOI: 10.1021/bi047772i [ACS Full Text], [CAS]
21. Pan, T.; Long, D. M.; Uhlenbeck, O. C. Divalent Metal Ions in RNA Folding and Catalysis. In *The RNA world: The nature of modern RNA suggests a prebiotic RNA world*; Gesteland, R. F.; Atkins, J. F., Eds.; Cold Spring Harbor Laboratory Press: Plainview, NY, **1993**; pp 271– 302.
22. Fedor, M. J.; Williamson, J. R.The Catalytic Diversity of RNAs *Nat. Rev. Mol. Cell Biol.* **2005**, 6, 399– 412, DOI: 10.1038/nrm1647 [CrossRef], [PubMed], [CAS]
23. Fedor, M. J.Comparative Enzymology and Structural Biology of RNA Self-Cleavage *Annu. Rev. Biophys.* **2009**, 38, 271– 299, DOI: 10.1146/annurev.biophys.050708.133710 [CrossRef], [PubMed], [CAS]
24. Cochrane, J. C.; Strobel, S. A.Catalytic Strategies of Self-Cleaving Ribozymes *Acc. Chem. Res.* **2008**, 41, 1027– 1035, DOI: 10.1021/ar800050c [ACS Full Text], [CAS]
25. Muller, S.; Appel, B.; Krellenberg, T.; Petkovic, S.The Many Faces of the Hairpin Ribozyme: Structural and Functional Variants of a Small Catalytic RNA *IUBMB Life* **2012**, 64, 36– 47, DOI: 10.1002/iub.575 [CrossRef], [PubMed], [CAS]
26. Lilley, D. M.Catalysis by the Nucleolytic Ribozymes *Biochem. Soc. Trans.* **2011**, 39, 641– 646, DOI: 10.1042/BST0390641 [CrossRef], [PubMed], [CAS]
27. Butcher, S. E.; Heckman, J. E.; Burke, J. M.Reconstitution of Hairpin Ribozyme Activity Following Separation of Functional Domains *J. Biol. Chem.* **1995**, 270, 29648– 29651, DOI: 10.1074/jbc.270.50.29648 [CrossRef], [PubMed], [CAS]
28. Hampel, K. J.; Walter, N. G.; Burke, J. M.The Solvent-Protected Core of the Hairpin Ribozyme-Substrate Complex *Biochemistry* **1998**, 37, 14672– 14682, DOI: 10.1021/bi981083n [ACS Full Text], [CAS]
29. Hampel, A.; Cowan, J. A.A Unique Mechanism for RNA Catalysis: the Role of Metal Cofactors in Hairpin Ribozyme Cleavage *Chem. Biol.* **1997**, 4, 513– 517, DOI: 10.1016/S1074-5521(97)90323-9 [CrossRef], [PubMed], [CAS]
30. Nesbitt, S.; Hegg, L. A.; Fedor, M. J.An Unusual pH-Independent and Metal-Ion-Independent Mechanism for Hairpin Ribozyme Catalysis *Chem. Biol.* **1997**, 4, 619– 630, DOI: 10.1016/S1074-5521(97)90247-7

[CrossRef], [PubMed], [CAS]

31. Young, K. J.; Gill, F.; Grasby, J. A.Metal Ions Play a Passive Role in the Hairpin Ribozyme Catalysed Reaction *Nucleic Acids Res.* **1997**, 25, 3760– 3766, DOI: 10.1093/nar/25.19.3760 [CrossRef], [PubMed], [CAS]
32. Walter, N. G.; Burker, J. M.The Hairpin Ribozyme: Structure, Assembly and Catalysis *Curr. Opin. Chem. Biol.* **1998**, 2, 24– 30, DOI: 10.1016/S1367-5931(98)80032-X [CrossRef], [PubMed], [CAS]
33. Fedor, M. J.Structure and Function of the Hairpin Ribozyme *J. Mol. Biol.* **2000**, 297, 269– 291, DOI: 10.1006/jmbi.2000.3560 [CrossRef], [PubMed], [CAS]
34. Fedor, M. J.The Catalytic Mechanism of the Hairpin Ribozyme *Biochem. Soc. Trans.* **2002**, 30, 1109– 1115, DOI: 10.1042/bst0301109 [CrossRef], [PubMed], [CAS]
35. Ferre-D'Amare, A. R.The Hairpin Ribozyme *Biopolymers* **2004**, 73, 71– 78, DOI: 10.1002/bip.10516 [CrossRef], [PubMed], [CAS]
36. Wilson, T. J.; Nahas, M.; Ha, T.; Lilley, D. M.Folding and Catalysis of the Hairpin Ribozyme *Biochem. Soc. Trans.* **2005**, 33, 461– 465, DOI: 10.1042/BST0330461 [CrossRef], [PubMed], [CAS]
37. Wilson, T. J.; Zhao, Z. Y.; Maxwell, K.; Kontogiannis, L.; Lilley, D. M.Importance of Specific Nucleotides in the Folding of the Natural Form of the Hairpin Ribozyme *Biochemistry* **2001**, 40, 2291– 2302, DOI: 10.1021/bi002644p [ACS Full Text], [CAS]
38. Wilson, T. J.; Lilley, D. M.Metal Ion Binding and the Folding of the Hairpin Ribozyme *RNA* **2002**, 8, 587– 600, DOI: 10.1017/S1355838202020514 [CrossRef], [PubMed], [CAS]
39. Lilley, D. M.A Chemo-Genetic Approach for the Study of Nucleobase Participation in Nucleolytic Ribozymes *Biol. Chem.* **2007**, 388, 699– 704, DOI: 10.1515/BC.2007.069 [CrossRef], [PubMed], [CAS]
40. Walter, N. G.; Hampel, K. J.; Brown, K. M.; Burke, J. M.Tertiary Structure Formation in the Hairpin Ribozyme Monitored by Fluorescence Resonance Energy Transfer *EMBO J.* **1998**, 17, 2378– 2391, DOI: 10.1093/emboj/17.8.2378 [CrossRef], [PubMed], [CAS]
41. Walter, N. G.; Chan, P. A.; Hampel, K. J.; Millar, D. P.; Burke, J. M.A Base Change in the Catalytic Core of the Hairpin Ribozyme Perturbs Function but Not Domain Docking *Biochemistry* **2001**, 40, 2580– 2587, DOI: 10.1021/bi001609f [ACS Full Text], [CAS]
42. Zhao, Z. Y.; Wilson, T. J.; Maxwell, K.; Lilley, D. M.The Folding of the Hairpin Ribozyme: Dependence on the Loops and the Junction *RNA* **2000**, 6, 1833– 1846, DOI: 10.1017/S1355838200001230 [CrossRef], [PubMed], [CAS]
43. Tan, E.; Wilson, T. J.; Nahas, M. K.; Clegg, R. M.; Lilley, D. M.; Ha, T.A Four-Way Junction Accelerates Hairpin Ribozyme Folding Via a Discrete Intermediate *Proc. Natl. Acad. Sci. U. S. A.* **2003**, 100, 9308– 9313, DOI: 10.1073/pnas.1233536100 [CrossRef], [PubMed], [CAS]
44. Klostermeier, D.; Millar, D. P.Helical Junctions As Determinants for RNA Folding: Origin of Tertiary Structure Stability of the Hairpin Ribozyme *Biochemistry* **2000**, 39, 12970– 12978, DOI: 10.1021/bi0014103 [ACS Full Text], [CAS]
45. Nahas, M. K.; Wilson, T. J.; Hohng, S.; Jarvie, K.; Lilley, D. M.; Ha, T.Observation of Internal Cleavage and Ligation Reactions of a Ribozyme *Nat. Struct. Mol. Biol.* **2004**, 11, 1107– 1113, DOI: 10.1038/nsmb842 [CrossRef], [PubMed], [CAS]
46. Wilson, T. J.; Nahas, M.; Araki, L.; Harusawa, S.; Ha, T.; Lilley, D. M.RNA Folding and the Origins of Catalytic Activity in the Hairpin Ribozyme *Blood Cells, Mol., Dis.* **2007**, 38, 8– 14, DOI: 10.1016/j.bcmd.2006.10.004 [CrossRef], [PubMed], [CAS]
47. Zhuang, X.; Kim, H.; Pereira, M. J.; Babcock, H. P.; Walter, N. G.; Chu, S.Correlating Structural Dynamics and Function in Single Ribozyme Molecules *Science* **2002**, 296, 1473– 1476, DOI: 10.1126/science.1069013 [CrossRef], [PubMed], [CAS]
48. Bokinsky, G.; Rueda, D.; Misra, V. K.; Rhodes, M. M.; Gordus, A.; Babcock, H. P.; Walter, N. G.; Zhuang, X.Single-Molecule Transition-State Analysis of RNA Folding *Proc. Natl. Acad. Sci. U. S. A.* **2003**, 100, 9302– 9307, DOI: 10.1073/pnas.1133280100 [CrossRef], [PubMed], [CAS]
49. Rueda, D.; Bokinsky, G.; Rhodes, M. M.; Rust, M. J.; Zhuang, X.; Walter, N. G.Single-Molecule Enzymology of RNA: Essential Functional Groups Impact Catalysis From a Distance *Proc. Natl. Acad. Sci. U. S. A.* **2004**, 101, 10066– 10071, DOI: 10.1073/pnas.0403575101 [CrossRef], [PubMed], [CAS]
50. Liu, S.; Bokinsky, G.; Walter, N. G.; Zhuang, X.Dissecting the Multistep Reaction Pathway of an RNA Enzyme by Single-Molecule Kinetic "Fingerprinting" *Proc. Natl. Acad. Sci. U. S. A.* **2007**, 104, 12634– 12639, DOI: 10.1073/pnas.0610597104 [CrossRef], [PubMed], [CAS]
51. Ditzler, M. A.; Rueda, D.; Mo, J.; Hakansson, K.; Walter, N. G.A Rugged Free Energy Landscape Separates Multiple Functional RNA Folds Throughout Denaturation *Nucleic Acids Res.* **2008**, 36, 7088– 7099, DOI: 10.1093/nar/gkn871 [CrossRef], [PubMed], [CAS]
52. Rhodes, M. M.; Reblova, K.; Sponer, J.; Walter, N. G.Trapped Water Molecules Are Essential to Structural Dynamics and Function of a Ribozyme *Proc. Natl. Acad. Sci. U. S. A.* **2006**, 103, 13380– 13385, DOI: 10.1073/pnas.0605090103 [CrossRef], [PubMed], [CAS]
53. McDowell, S. E.; Spackova, N.; Sponer, J.; Walter, N. G.Molecular Dynamics Simulations of RNA: an in Silico Single Molecule Approach *Biopolymers* **2007**, 85, 169– 184, DOI: 10.1002/bip.20620 [CrossRef], [PubMed], [CAS]
54. Ditzler, M. A.; Sponer, J.; Walter, N. G.Molecular Dynamics Suggest Multifunctionality of an Adenine Imino Group in Acid-Base Catalysis of the Hairpin Ribozyme *RNA* **2009**, 15, 560– 575, DOI: 10.1261/rna.1416709 [CrossRef], [PubMed], [CAS]
55. Ditzler, M. A.; Otyepka, M.; Sponer, J.; Walter, N. G.Molecular Dynamics and Quantum Mechanics of RNA: Conformational and Chemical Change We Can Believe *Acc. Chem. Res.* **2010**, 43, 40– 47, DOI: 10.1021/ar900093g [ACS Full Text], [CAS]
56. Mlynsky, V.; Banas, P.; Hollas, D.; Reblova, K.; Walter, N. G.; Sponer, J.; Otyepka, M.Extensive Molecular Dynamics Simulations Showing That Canonical G8 and Protonated A38H+ Forms Are Most Consistent With Crystal Structures of Hairpin Ribozyme *J. Phys. Chem. B* **2010**, 114, 6642– 6652, DOI: 10.1021/jp1001258 [ACS Full Text], [CAS]
57. Mlynsky, V.; Banas, P.; Walter, N. G.; Sponer, J.; Otyepka, M.QM/MM Studies of Hairpin Ribozyme Self-Cleavage Suggest the Feasibility of Multiple Competing Reaction Mechanisms *J. Phys. Chem. B* **2011**, 115, 13911– 13924, DOI: 10.1021/jp206963g [ACS Full Text], [CAS]
58. Kath-Schorr, S.; Wilson, T. J.; Li, N. S.; Lu, J.; Piccirilli, J. A.; Lilley, D. M.General Acid-Base Catalysis Mediated by Nucleobases in the Hairpin Ribozyme *J. Am. Chem. Soc.* **2012**, 134, 16717– 16724, DOI: 10.1021/ja3067429 [ACS Full Text], [CAS]
59. Mlynsky, V.; Banas, P.; Sponer, J.; van der Kamp, M. W.; Mulholland, A. J.; Otyepka, M.Comparison of Ab Initio, DFT, and Semiempirical QM/MM Approaches for Description of Catalytic Mechanism of Hairpin

Ribozyme *J. Chem. Theory Comput.* **2014**, 10, 1608– 1622, DOI: 10.1021/ct401015e [ACS Full Text], [CAS]

60. Mlynsky, V.; Kuhrova, P.; Zgarbova, M.; Jurecka, P.; Walter, N. G.; Otyepka, M.; Sponer, J.; Banas, P.Reactive Conformation of the Active Site in the Hairpin Ribozyme Achieved by Molecular Dynamics Simulations With Epsilon/Zeta Force Field Reparametrizations *J. Phys. Chem. B* **2015**, 119, 4220– 4229, DOI: 10.1021/jp512069n [ACS Full Text], [CAS]
61. Mlynsky, V.; Walter, N. G.; Sponer, J.; Otyepka, M.; Banas, P.The Role of an Active Site Mg(2+) in HDV Ribozyme Self-Cleavage: Insights From QM/MM Calculations *Phys. Chem. Chem. Phys.* **2015**, 17, 670– 679, DOI: 10.1039/C4CP03857F [CrossRef], [PubMed], [CAS]
62. Heldenbrand, H.; Janowski, P. A.; Giambasu, G.; Giese, T. J.; Wedekind, J. E.; York, D. M.Evidence for the Role of Active Site Residues in the Hairpin Ribozyme From Molecular Simulations Along the Reaction Path *J. Am. Chem. Soc.* **2014**, 136, 7789– 7792, DOI: 10.1021/ja500180q [ACS Full Text], [CAS]
63. Cai, Z.; Tinoco, I., Jr.Solution Structure of Loop A From the Hairpin Ribozyme From Tobacco Ringspot Virus Satellite *Biochemistry* **1996**, 35, 6026– 6036, DOI: 10.1021/bi952985g [ACS Full Text], [CAS]
64. Butcher, S. E.; Allain, F. H.; Feigon, J.Solution Structure of the Loop B Domain From the Hairpin Ribozyme *Nat. Struct. Biol.* **1999**, 6, 212– 216, DOI: 10.1038/6651 [CrossRef], [PubMed], [CAS]
65. Rupert, P. B.; Ferre-D'Amare, A. R.Crystal Structure of a Hairpin Ribozyme-Inhibitor Complex With Implications for Catalysis *Nature* **2001**, 410, 780– 786, DOI: 10.1038/35071009 [CrossRef], [PubMed], [CAS]
66. Rupert, P. B.; Massey, A. P.; Sigurdsson, S.; Ferré-D'Amaré, A. R.Transition State Stabilization by a Catalytic RNA *Science* **2002**, 298, 1421– 1424, DOI: 10.1126/science.1076093 [CrossRef], [PubMed], [CAS]
67. Alam, S.; Grum-Tokars, V.; Krucinska, J.; Kundracik, M. L.; Wedekind, J. E.Conformational Heterogeneity at Position U37 of an All-RNA Hairpin Ribozyme With Implications for Metal Binding and the Catalytic Structure of the S-Turn *Biochemistry* **2005**, 44, 14396– 14408, DOI: 10.1021/bi051550i [ACS Full Text], [CAS]
68. Salter, J.; Krucinska, J.; Alam, S.; Grum-Tokars, V.; Wedekind, J. E.Water in the Active Site of an All-RNA Hairpin Ribozyme and Effects of Gua8 Base Variants on the Geometry of Phosphoryl Transfer *Biochemistry* **2006**, 45, 686– 700, DOI: 10.1021/bi051887k [ACS Full Text], [CAS]
69. MacElrevey, C.; Salter, J. D.; Krucinska, J.; Wedekind, J. E.Structural Effects of Nucleobase Variations at Key Active Site Residue Ade38 in the Hairpin Ribozyme *RNA* **2008**, 14, 1600– 1616, DOI: 10.1261/rna.1055308 [CrossRef], [PubMed], [CAS]
70. Spitale, R. C.; Volpini, R.; Mungillo, M. V.; Krucinska, J.; Cristalli, G.; Wedekind, J. E.Single-Atom Imino Substitutions at A9 and A10 Reveal Distinct Effects on the Fold and Function of the Hairpin Ribozyme Catalytic Core *Biochemistry* **2009**, 48, 7777– 7779, DOI: 10.1021/bi9011622 [ACS Full Text], [CAS]
71. Liberman, J. A.; Guo, M.; Jenkins, J. L.; Krucinska, J.; Chen, Y.; Carey, P. R.; Wedekind, J. E.A Transition-State Interaction Shifts Nucleobase Ionization Toward Neutrality To Facilitate Small Ribozyme Catalysis *J. Am. Chem. Soc.* **2012**, 134, 16933– 16936, DOI: 10.1021/ja3070528 [ACS Full Text], [CAS]
72. Ferre-D'Amare, A. R.; Rupert, P. B.The Hairpin Ribozyme: From Crystal Structure to Function *Biochem. Soc. Trans.* **2002**, 30, 1105– 1109, DOI: 10.1042/bst0301105 [CrossRef], [PubMed], [CAS]
73. Pinard, R.; Lambert, D.; Walter, N. G.; Heckman, J. E.; Major, F.; Burke, J. M.Structural Basis for the Guanosine Requirement of the Hairpin Ribozyme *Biochemistry* **1999**, 38, 16035– 16039, DOI: 10.1021/bi992024s [ACS Full Text], [CAS]
74. Hampel, K. J.; Burke, J. M.A Conformational Change in the "Loop E-Like" Motif of the Hairpin Ribozyme Is Coincidental With Domain Docking and Is Essential for Catalysis *Biochemistry* **2001**, 40, 3723– 3729, DOI: 10.1021/bi0028385 [ACS Full Text], [CAS]
75. Ferre-D'Amare, A. R.The Hairpin Ribozyme *Biopolymers* **2004**, 73, 71– 78, DOI: 10.1002/bip.10516 [CrossRef], [PubMed], [CAS]
76. Sumita, M.; White, N. A.; Julien, K. R.; Hoogstraten, C. G.Intermolecular Domain Docking in the Hairpin Ribozyme: Metal Dependence, Binding Kinetics, and Catalysis *RNA Biol.* **2013**, 10, 425– 435, DOI: 10.4161/rna.23609 [CrossRef], [PubMed], [CAS]
77. Clore, G. M.; Kuszewski, J.Improving the Accuracy of NMR Structures of RNA by Means of Conformational Database Potentials of Mean Force As Assessed by Complete Dipolar Coupling Cross-Validation *J. Am. Chem. Soc.* **2003**, 125, 1518– 1525, DOI: 10.1021/ja028383j [ACS Full Text], [CAS]
78. Feig, M.; Karanicolas, J.; Brooks, C. L., IIIMMTSB Tool Set: Enhanced Sampling and Multiscale Modeling Methods for Applications in Structural Biology *J. Mol. Graphics Modell.* **2004**, 22, 377– 395, DOI: 10.1016/j.jmgm.2003.12.005 [CrossRef], [PubMed], [CAS]
79. Bowman, G. R.; Huang, X. H.; Pande, V. S.Using Generalized Ensemble Simulations and Markov State Models to Identify Conformational States *Methods* **2009**, 49, 197– 201, DOI: 10.1016/j.ymeth.2009.04.013 [CrossRef], [PubMed], [CAS]
80. Beauchamp, K. A.; Bowman, G. R.; Lane, T. J.; Maibaum, L.; Haque, I. S.; Pande, V. S.MSMBuilder2: Modeling Conformational Dynamics on the Picosecond to Millisecond Scale *J. Chem. Theory Comput.* **2011**, 7, 3412– 3419, DOI: 10.1021/ct200463m [ACS Full Text], [CAS]
81. Cornell, W. D.; Cieplak, P.; Bayly, C. I.; Gould, I. R.; Merz, K. M.; Ferguson, D. M.; Spellmeyer, D. C.; Fox, T.; Caldwell, J. W.; Kollman, P. A.A Second Generation Force Field for the Simulation of Proteins, Nucleic Acids, and Organic Molecules (Vol 117, Pg 5179, 1995) *J. Am. Chem. Soc.* **1996**, 118, 2309, DOI: 10.1021/ja955032e [ACS Full Text], [CAS]
82. Cheatham, T. E.; Cieplak, P.; Kollman, P. A.A Modified Version of the Cornell Et Al. Force Field With Improved Sugar Pucker Phases and Helical Repeat *J. Biomol. Struct. Dyn.* **1999**, 16, 845– 862, DOI: 10.1080/07391102.1999.10508297 [CrossRef], [PubMed], [CAS]
83. Perez, A.; Marchan, I.; Svozil, D.; Sponer, J.; Cheatham, T. E., III; Laughton, C. A.; Orozco, M.Refinement of the AMBER Force Field for Nucleic Acids: Improving the Description of Alpha/Gamma Conformers *Biophys. J.* **2007**, 92, 3817– 3829, DOI: 10.1529/biophysj.106.097782 [CrossRef], [PubMed], [CAS]
84. Foloppe, N.; MacKerell, A. D.All-Atom Empirical Force Field for Nucleic Acids: I. Parameter Optimization Based on Small Molecule and Condensed Phase Macromolecular Target Data *J. Comput. Chem.* **2000**, 21, 86– 104, DOI: 10.1002/(SICI)1096-987X(20000130)21:2<86::AID-JCC2>3.0.CO;2-G [CrossRef], [CAS]
85. MacKerell, A. D.; Banavali, N. K.All-Atom Empirical Force Field for Nucleic Acids: II. Application to Molecular Dynamics Simulations of DNA and RNA in Solution *J. Comput. Chem.* **2000**, 21, 105– 120, DOI: 10.1002/(SICI)1096-987X(20000130)21:2<105::AID-JCC3>3.0.CO;2-P [CrossRef], [CAS]
86. Best, R. B.; Zhu, X.; Shim, J.; Lopes, P. E.; Mittal, J.; Feig, M.; Mackerell, A. D., Jr.Optimization of the Additive CHARMM All-Atom Protein Force Field Targeting Improved Sampling of the Backbone Phi, Psi and Side-Chain Chi(1) and Chi(2) Dihedral Angles *J. Chem. Theory Comput.* **2012**, 8, 3257– 3273, DOI: 10.1021/ct300400x [ACS Full Text], [CAS]

87. MacKerell, A. D.; Bashford, D.; Bellott, M.; Dunbrack, R. L.; Evanseck, J. D.; Field, M. J.; Fischer, S.; Gao, J.; Guo, H.; Ha, S., et al. All-Atom Empirical Potential for Molecular Modeling and Dynamics Studies of Proteins *J. Phys. Chem. B* **1998**, 102, 3586– 3616, DOI: 10.1021/jp973084f [ACS Full Text], [CAS]

88. Huang, J.; Mackerell, A. D., Jr.CHARMM36 All-Atom Additive Protein Force Field: Validation Based on Comparison to NMR Data *J. Comput. Chem.* **2013**, 34, 2135– 2145, DOI: 10.1002/jcc.23354 [CrossRef], [PubMed], [CAS]

89. Besseova, I.; Banas, P.; Kuhrova, P.; Kosinova, P.; Otyepka, M.; Sponer, J.Simulations of A-RNA Duplexes. The Effect of Sequence, Solute Force Field, Water Model, and Salt Concentration *J. Phys. Chem. B* **2012**, 116, 9899– 9916, DOI: 10.1021/jp3014817 [ACS Full Text], [CAS]

90. Bergonzo, C.; Henriksen, N. M.; Roe, D. R.; Cheatham, T. E., IIIHighly Sampled Tetranucleotide and Tetraloop Motifs Enable Evaluation of Common RNA Force Fields *RNA* **2015**, 21, 1578– 1590, DOI: 10.1261/rna.051102.115 [CrossRef], [PubMed], [CAS]

91. Shieh, F. K.; Youngblood, B.; Reich, N. O.The Role of Arg165 Towards Base Flipping, Base Stabilization and Catalysis in M.HhaI *J. Mol. Biol.* **2006**, 362, 516– 527, DOI: 10.1016/j.jmb.2006.07.030 [CrossRef], [PubMed], [CAS]

92. Johnson, J. E., Jr.; Hoogstraten, C. G.Extensive Backbone Dynamics in the GCAA RNA Tetraloop Analyzed Using ^{13}C NMR Spin Relaxation and Specific Isotope Labeling *J. Am. Chem. Soc.* **2008**, 130, 16757– 16769, DOI: 10.1021/ja805759z [ACS Full Text], [CAS]

93. Hoogstraten, C. G.; Wank, J. R.; Pardi, A.Active Site Dynamics in the Lead-Dependent Ribozyme *Biochemistry* **2000**, 39, 9951– 9958, DOI: 10.1021/bi0007627 [ACS Full Text], [CAS]

94. Blad, H.; Reiter, N. J.; Abildgaard, F.; Markley, J. L.; Butcher, S. E.Dynamics and Metal Ion Binding in the U6 RNA Intramolecular Stem-Loop As Analyzed by NMR *J. Mol. Biol.* **2005**, 353, 540– 555, DOI: 10.1016/j.jmb.2005.08.030 [CrossRef], [PubMed], [CAS]

95. Grum-Tokars, V.; Milovanovic, M.; Wedekind, J. E.Crystallization and X-Ray Diffraction Analysis of an All-RNA U_{39}C Mutant of the Minimal Hairpin Ribozyme *Acta Crystallogr., Sect. D: Biol. Crystallogr.* **2003**, 59, 142– 145, DOI: 10.1107/S0907444902019066 [CrossRef], [PubMed], [CAS]

96. Torelli, A. T.; Krucinska, J.; Wedekind, J. E.A Comparison of Vanadate to a 2′-5′ Linkage at the Active Site of a Small Ribozyme Suggests a Role for Water in Transition-State Stabilization *RNA* **2007**, 13, 1052– 1070, DOI: 10.1261/rna.510807 [CrossRef], [PubMed], [CAS]

97. Spitale, R. C.; Volpini, R.; Heller, M. G.; Krucinska, J.; Cristalli, G.; Wedekind, J. E.Identification of an Imino Group Indispensable for Cleavage by a Small Ribozyme *J. Am. Chem. Soc.* **2009**, 131, 6093– 6095, DOI: 10.1021/ja900450h [ACS Full Text], [CAS]

98. Torres, R. A.; Bruice, T. C.The Mechanism of Phosphodiester Hydrolysis: Near in-Line Attack Conformations in the Hammerhead Ribozyme *J. Am. Chem. Soc.* **2000**, 122, 781– 791, DOI: 10.1021/ja993094p [ACS Full Text], [CAS]

99. Mir, A.; Chen, J.; Robinson, K.; Lendy, E.; Goodman, J.; Neau, D.; Golden, B. L.Two Divalent Metal Ions and Conformational Changes Play Roles in the Hammerhead Ribozyme Cleavage Reaction *Biochemistry* **2015**, 54, 6369– 6381, DOI: 10.1021/acs.biochem.5b00824 [ACS Full Text], [CAS]

100. Gaines, C. S.; York, D. M.Ribozyme Catalysis With a Twist: Active State of the Twister Ribozyme in Solution Predicted From Molecular Simulation *J. Am. Chem. Soc.* **2016**, 138, 3058– 3065, DOI: 10.1021/jacs.5b12061 [ACS Full Text], [CAS]

101. Lee, T.-S.; Radak, B. K.; Harris, M. E.; York, D. M.A Two-Metal-Ion-Mediated Conformational Switching Pathway for HDV Ribozyme Activation *ACS Catal.* **2016**, 6, 1853– 1869, DOI: 10.1021/acscatal.5b02158 [ACS Full Text], [CAS]

102. Kurisaki, I.; Takayanagi, M.; Nagaoka, M.Combined Mechanism of Conformational Selection and Induced Fit in U1A-RNA Molecular Recognition *Biochemistry* **2014**, 53, 3646– 3657, DOI: 10.1021/bi401708q [ACS Full Text], [CAS]

103. Jucker, F. M.; Heus, H. A.; Yip, P. F.; Moors, E. H. M.; Pardi, A.A Network of Heterogeneous Hydrogen Bonds in GNRA Tetraloops *J. Mol. Biol.* **1996**, 264, 968– 980, DOI: 10.1006/jmbi.1996.0690 [CrossRef], [PubMed], [CAS]

104. Sorin, E. J.; Engelhardt, M. A.; Herschlag, D.; Pande, V. S.RNA Simulations: Probing Hairpin Unfolding and the Dynamics of a GNRA Tetraloop *J. Mol. Biol.* **2002**, 317, 493– 506, DOI: 10.1006/jmbi.2002.5447 [CrossRef], [PubMed], [CAS]

105. Zichi, D. A.Molecular-Dynamics of Rna With the Opls Force-Field - Aqueous Simulation of A Hairpin Containing A Tetranucleotide Loop *J. Am. Chem. Soc.* **1995**, 117, 2957– 2969, DOI: 10.1021/ja00116a001 [ACS Full Text], [CAS]

106. Chen, G.; Znosko, B. M.; Jiao, X.; Turner, D. H.Factors Affecting Thermodynamic Stabilities of RNA 3 × 3 Internal Loops *Biochemistry* **2004**, 43, 12865– 12876, DOI: 10.1021/bi049168d [ACS Full Text], [CAS]

107. SantaLucia, J.; Kierzek, R.; Turner, D. H.Functional-Group Substitutions As Probes of Hydrogen-Bonding Between GA Mismatches in RNA Internal Loops *J. Am. Chem. Soc.* **1991**, 113, 4313– 4322, DOI: 10.1021/ja00011a039 [ACS Full Text], [CAS]

108. Schroeder, S. J.; Turner, D. H.Factors Affecting the Thermodynamic Stability of Small Asymmetric Internal Loops in RNA *Biochemistry* **2000**, 39, 9257– 9274, DOI: 10.1021/bi000229r [ACS Full Text], [CAS]

109. Znosko, B. M.; Burkard, M. E.; Schroeder, S. J.; Krugh, T. R.; Turner, D. H.Sheared A(Anti)·A(Anti) Base Pairs in a Destabilizing 2 × 2 Internal Loop: The NMR Structure of 5 ′(RGGCAAGCCU)(2) *Biochemistry* **2002**, 41, 14969– 14977, DOI: 10.1021/bi020326f [ACS Full Text], [CAS]

110. Al-Hashimi, H. M.Beyond Static Structures of RNA by NMR: Folding, Refolding, and Dynamics at Atomic Resolution *Biopolymers* **2007**, 86, 345– 347, DOI: 10.1002/bip.20754 [CrossRef], [PubMed], [CAS]

111. Dethoff, E. A.; Chugh, J.; Mustoe, A. M.; Al-Hashimi, H. M.Functional Complexity and Regulation Through RNA Dynamics *Nature* **2012**, 482, 322– 330, DOI: 10.1038/nature10885 [CrossRef], [PubMed], [CAS]

112. Sun, X.; Zhang, Q.; Al-Hashimi, H. M.Resolving Fast and Slow Motions in the Internal Loop Containing Stem-Loop 1 of HIV-1 That Are Modulated by Mg2+ Binding: Role in the Kissing-Duplex Structural Transition *Nucleic Acids Res.* **2007**, 35, 1698– 1713, DOI: 10.1093/nar/gkm020 [CrossRef], [PubMed], [CAS]

113. Lambert, D.; Heckman, J. E.; Burke, J. M.Cation-Specific Structural Accommodation Within a Catalytic RNA *Biochemistry* **2006**, 45, 829– 838, DOI: 10.1021/bi0513709 [ACS Full Text], [CAS]

114. Kraemer-Chant, C. M.; Heckman, J. E.; Lambert, D.; Burke, J. M.Cobalt(III)Hexaammine-Dependent Photocrosslinks in the Hairpin Ribozyme *J. Inorg. Biochem.* **2014**, 131, 87– 98, DOI: 10.1016/j.jinorgbio.2013.11.001 [CrossRef], [PubMed], [CAS]

115. Sargueil, B.; Hampel, K. J.; Lambert, D.; Burke, J. M.In Vitro Selection of Second Site Revertants Analysis of the Hairpin Ribozyme Active Site *J. Biol. Chem.* **2003**, 278, 52783– 52791, DOI: 10.1074/jbc.M306703200 [CrossRef], [PubMed], [CAS]

116. Bailor, M. H.; Mustoe, A. M.; Brooks, C. L., III; Al-Hashimi, H. M.Topological Constraints: Using RNA Secondary Structure to Model 3D Conformation, Folding Pathways, and Dynamic Adaptation *Curr. Opin. Struct. Biol.* **2011**, 21, 296– 305, DOI: 10.1016/j.sbi.2011.03.009 [CrossRef], [PubMed], [CAS]

117. Schultes, E. A.; Spasic, A.; Mohanty, U.; Bartel, D. P.Compact and Ordered Collapse of Randomly Generated RNA Sequences *Nat. Struct. Mol. Biol.* **2005**, 12, 1130– 1136, DOI: 10.1038/nsmb1014 [CrossRef], [PubMed], [CAS]

118. Hoogstraten, C. G.; Johnson, J. E., Jr.Metabolic Labeling: Taking Advantage of Bacterial Pathways to Prepare Spectroscopically Useful Isotope Patterns in Proteins and Nucleic Acids *Concepts Magn. Reson., Part A* **2008**, 32, 34– 55, DOI: 10.1002/cmr.a.20103 [CrossRef], [CAS]

119. Delano, W. L. *The PyMOL Molecular Graphics System*; DeLano Scientific: Palo Alto, CA, USA, **2002**.

120. Humphrey, W.; Dalke, A.; Schulten, K.VMD: Visual Molecular Dynamics *J. Mol. Graphics* **1996**, 14, 33– 38, DOI: 10.1016/0263-7855(96)00018-5 [CrossRef], [PubMed], [CAS]